

TOWARDS ALIGNED LAYOUT GENERATION VIA DIFFUSION MODEL WITH AESTHETIC CONSTRAINTS

Jian Chen¹, Ruiyi Zhang², Yufan Zhou², Rajiv Jain², Zhiqiang Xu³

Ryan Rossi², Changyou Chen¹

University at Buffalo¹, Adobe Research², MBZUAI³

{jchen378, changyou}@buffalo.edu, ruiyizhang@adobe.com

ABSTRACT

Controllable layout generation refers to the process of creating a plausible visual arrangement of elements within a graphic design (*e.g.*, document and web designs) with constraints representing design intentions. Although recent diffusion-based models have achieved state-of-the-art FID scores, they tend to exhibit more pronounced misalignment compared to earlier transformer-based models. In this work, we propose the **L**ayout **C**onstraint **d**iffusion **m**odel (**LACE**)¹, a unified model to handle a broad range of layout generation tasks, such as arranging elements with specified attributes and refining or completing a coarse layout design. The model is based on continuous diffusion models. Compared with existing methods that use discrete diffusion models, continuous state-space design can enable the incorporation of differentiable aesthetic constraint functions in training. For conditional generation, we introduce conditions via masked input. Extensive experiment results show that **LACE** produces high-quality layouts and outperforms existing state-of-the-art baselines.

1 INTRODUCTION

Leveraging advanced algorithms and artificial intelligence, automated layout generation serves as a cost-effective and scalable tool that facilitates a diverse range of applications including website development (Pang et al., 2016), UI design (Deka et al., 2017), urban planning (Yang et al., 2013), and editing in printed media (Zhong et al., 2019). Layout generation tasks fall into either unconditional or conditional categories. Unconditional generation refers to the process where layouts are generated from scratch without predefined conditions or constraints. Conditional generation, on the other hand, is guided by user specification, such as element types, positions and sizes, or unfinished layouts, allowing for more controlled and targeted results.

Previous research utilized generative models such as GANs (Goodfellow et al., 2014; Kikuchi et al., 2021), VAEs (Kingma & Welling, 2013), and transformer-based (Vaswani et al., 2017; Kong et al., 2022) models. Recent studies, however, have shifted the focus towards the application of diffusion models for better generative quality and versatility in conditional generation (Hui et al., 2023).

Diffusion-based models handle layout attributes as discrete or continuous variables and corrupt the data using categorical and Gaussian noise based on the discrete (Austin et al., 2021) and continuous (Ho et al., 2020) diffusion frameworks. These different corruption mechanisms result in distinct patterns during the generation process, as illustrated in Figure 1. Discrete diffusion, starting from a blank canvas, generates elements incrementally. Emerged elements tend to remain static, thus limiting the model’s ability to make global adjustments. Continuous diffusion, by contrast, starts with a random arrangement and refines it to an organized one over time, which is arguably more flexible in modeling.

Diffusion models, while achieving state-of-the-art FID scores, usually underperform in terms of alignment and MaxIoU scores compared to earlier transformer-based models (Gupta et al., 2021), especially in unconditional generation (Inoue et al., 2023). These metrics can be leveraged for constraint optimization in continuous diffusion models to enhance layout aesthetics. However, due to

¹Code is available at <https://github.com/puar-playground/LACE>



Figure 1: Comparisons of latent states in continuous and discrete diffusion for layout generation. Discrete diffusion adds elements to a blank canvas incrementally, and the added elements remain fixed. Continuous diffusion gradually refines a random layout into an organized one over time.

the non-differentiability of quantized geometric attributes, discrete models miss out on this optimization potential. On the other hand, continuous diffusion models face challenges in task unification because the sample spaces of Gaussian distribution and the data distribution (canvas range and probability simplex) are different. In contrast to discrete diffusion models (Inoue et al., 2023; Hui et al., 2023), which can direct unconditional models to meet conditional goals by masking specific attributes, this strategy proves inefficient for continuous models. This limitation could explain why earlier research on continuous diffusion models (Chai et al., 2023; He et al., 2023) focused on a single layout generation task.

In this study, we introduce the LAyout Constraint Diffusion modEl (LACE). A unified model designed to generate both geometric and categorical attributes for various tasks in a continuous space. While the neural network is trained to predict noise following the classic DDPM framework (He et al., 2023), we employ a simple reparameterization technique to compute a layout prediction (Song et al., 2020). This prediction then serves as a target to apply differentiable aesthetic constraint functions, thereby enhancing the model performance. In addition, we designed a global alignment loss and a pairwise overlap loss that serve as constraint functions during the training and post-processing stages. Global alignment loss promotes the learning of alignment patterns from real data during training and is used to refine global alignment in the post-processing stage. We train models with masked input to unify unconditional and conditional generation, following an approach similar to masked autoencoders, as seen in DiffMAE (Wei et al., 2023). To avoid convergence to the local minimum introduced by the constraints, we propose a time-dependent weight to deactivate the constraints for noisier time steps.

Our contribution is summarized as:

- Built upon a diffusion model, we formulate various controllable layout generation tasks as conditional generation processes in continuous space, enabling constraint optimization for enhanced quality.
- We propose two aesthetic constraint loss functions that promote global alignment and minimize overlap in the layout. These functions serve as constraints during both the training and post-processing phases.
- We conducted extensive experiments and achieved state-of-the-art results on public benchmarks across various layout generation tasks.

2 METHODOLOGY

2.1 PRELIMINARY: CONTINUOUS DIFFUSION MODELS

Diffusion models (Ho et al., 2020) are generative models characterized by a forward and reverse Markov process. In the forward process, a continuous valued data-point \mathbf{x}_0 is gradually corrupted to intermediate noisy latents $\mathbf{x}_{1:T}$, which converges to a random variable of the standard multi-variate Gaussian distribution $\mathcal{N}(0, \mathbf{I})$ after T steps. The transition steps between adjacent intermediate predictions is modeled as Gaussian distributions, $q(\mathbf{x}_t|\mathbf{x}_{t-1}) = \mathcal{N}(\mathbf{x}_t; \sqrt{1 - \beta_t} \mathbf{x}_{t-1}, \beta_t \mathbf{I})$, with

a variance schedule β_1, \dots, β_T . The forward process admits a closed-form sampling distribution, $q(\mathbf{x}_t | \mathbf{x}_0) = \mathcal{N}(\mathbf{x}_t; \sqrt{\bar{\alpha}_t} \mathbf{x}_0, (1 - \bar{\alpha}_t) \mathbf{I})$ at arbitrary timestep t , where $\bar{\alpha}_t = \prod_{s=1}^t \alpha_s$ and $\alpha_t = (1 - \beta_t)$.

In the reverse (generative) process, the data \mathbf{x}_0 is reconstructed gradually by sampling from a series of estimated transition distributions $p_\theta(\mathbf{x}_{t-1} | \mathbf{x}_t)$ start from a standard Gaussian random variable $X_T \sim \mathcal{N}(0, \mathbf{I})$. The transition distributions are learned by optimizing the evidence lower bound consists of a series of KL-divergence:

$$\mathbb{E}_q \left[D_{\text{KL}}(q(\mathbf{x}_T | \mathbf{x}_0) || p(\mathbf{x}_T)) + \sum_{t>1}^T D_{\text{KL}}(q(\mathbf{x}_{t-1} | \mathbf{x}_t, \mathbf{x}_0) || p_\theta(\mathbf{x}_{t-1} | \mathbf{x}_t)) - \log p_\theta(\mathbf{x}_0 | \mathbf{x}_1) \right]. \quad (1)$$

Since the posterior distributions $q(\mathbf{x}_{t-1} | \mathbf{x}_t, \mathbf{x}_0)$ are also Gaussian for an infinitesimal variance β_t (Feller, 2015) and can be approximated by \mathbf{x}_0 -parameterization (Song et al., 2020) as:

$$q(\mathbf{x}_{t-1} | \mathbf{x}_t, \mathbf{x}_0) = \mathcal{N}(\mathbf{x}_{t-1}; \tilde{\mu}(\mathbf{x}_t, t), \tilde{\beta}_t \mathbf{I}) \quad (2)$$

$$\text{where } \tilde{\mu}(\mathbf{x}_t, t) = \frac{1}{\sqrt{\alpha_t}} \left(\mathbf{x}_t - \frac{\beta_t}{\sqrt{1 - \bar{\alpha}_t}} \epsilon \right), \quad \epsilon \sim \mathcal{N}(0, \mathbf{I}) \quad \text{and} \quad \tilde{\beta}_t = \frac{1 - \bar{\alpha}_{t-1}}{1 - \bar{\alpha}_t} \beta_t, \quad (3)$$

the transition distributions could be estimated as a Gaussian with a mean:

$$\mu_\theta(\mathbf{x}_t, t) = \frac{1}{\sqrt{\alpha_t}} \left(\mathbf{x}_t - \frac{\beta_t}{\sqrt{1 - \bar{\alpha}_t}} \epsilon_\theta(\mathbf{x}_t, t) \right), \quad (4)$$

where ϵ_θ is a function approximator and is usually trained using a simplified objective:

$$\mathcal{L}_{\text{simple}} = \|\epsilon - \tilde{\epsilon}_\theta(\sqrt{\bar{\alpha}_t} \mathbf{x}_0 + \sqrt{1 - \bar{\alpha}_t} \epsilon, t)\|^2, \quad (5)$$

where $\epsilon \sim \mathcal{N}(0, \mathbf{I})$.

2.2 CONTINUOUS LAYOUT GENERATION

Similar to previous work (Inoue et al., 2023; Chai et al., 2023; He et al., 2023), we define a layout with l elements as $\mathbf{x} = \{(c_i, \mathbf{b}_i), \dots, (c_l, \mathbf{b}_l)\}$, where $c_i \in \{0, 1, \dots, N - 1\}$ and $\mathbf{b}_i \in [0, 1]^4$ is the label (spanning N classes) and the bounding box for the i -th element. The bounding box is defined by its center coordinates (x, y) and sizes ratio (width, height). In order to allow variable length generation, we extend layouts to a uniform length L with padding elements, which has an extra class label $c = N$ and a bounding box initialized to zero, denoted as $b = (0, 0, 0, 0)$. Consequently, any layout within a dataset of N classes is represented as a vector sequence with $N + 5$ dimensions and a length of L .

In contrast to previous discrete diffusion (Austin et al., 2021) based methods that quantize bounding box attributes to discrete bins, our approach considers them as continuous size and position ratio ranging from 0 to 1. This shift towards continuous variables enables the integration of continuous constraint functions to optimize aesthetic qualities. Moreover, following previous work (Han et al., 2022), we employ continuous label vectors of $(N + 1)$ dimension to represent noisy classification logits. In other words, label vectors are not confined in the probability simplex when $t > 0$. However, the clean data at $t = 0$ still has a one-hot label vectors. This design allows direct application of the classic diffusion model using Gaussian noise (Ho et al., 2020) without modality-wise corruption tricks (Hui et al., 2023; Inoue et al., 2023). An example is shown in Figure 2.

Conditional Generation Instead of training separate models for unconditional and various conditional generation, we train a single neural network to handle multiple generation tasks. In training, we employ three types of binary condition masks as data augmentation that fix the label, size attributes of all elements or all attributes of partial elements. Specifically, given a binary condition mask \mathbf{m} , the noisy latent is augmented as $\hat{\mathbf{x}}_t = \mathbf{m} \circ \mathbf{x}_0 + (\mathbf{1} - \mathbf{m}) \circ \mathbf{x}_t$, where $\mathbf{1}$ denotes a all-ones matrix.

2.3 RECONSTRUCTION AND AESTHETIC CONSTRAINTS

Following recent work, we introduce a reconstruction loss to encourage plausible predictions of \mathbf{x}_0 at each time step (Austin et al., 2021; Hui et al., 2023). Thus, the total loss is defined as $\mathcal{L} = \mathcal{L}_{\text{simple}} + \mathcal{L}_{\text{rec}}$.

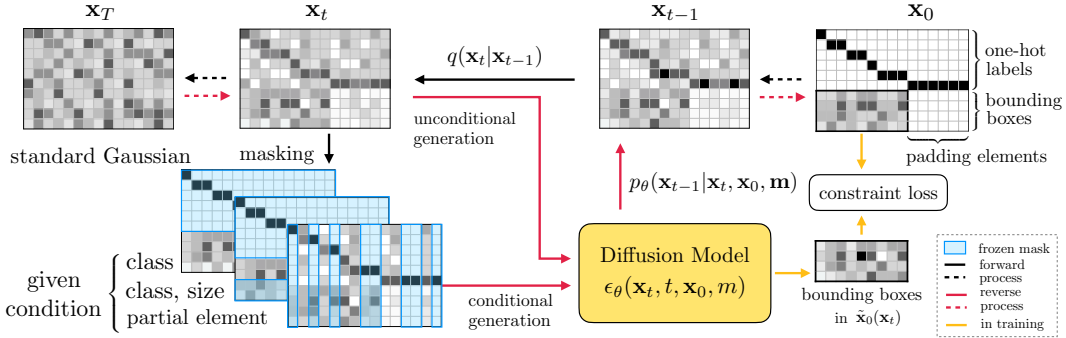


Figure 2: Overview of the layout generation model: The figure shows a layout generation of up to 15 elements from 5 classes. The layout is padded for consistency using padding elements, represented by an extra class in the 6-dimensional one-hot vector. The bounding box uses a 4-dimensional continuous vector. Dashed lines represent multi-step processes and solid lines represent a single step. The forward process corrupt data with Gaussian noise, while the reverse process trains a neural network to denoise the noisy latent \mathbf{x}_t and its three augmentations using condition masks. Predicted bounding boxes is used to compute constraint loss against real ones.

Specifically, by rewriting the closed-form sampling distribution for the forward process, we have $\mathbf{x}_t = \sqrt{\bar{\alpha}_t} \mathbf{x}_0 + \sqrt{1 - \bar{\alpha}_t} \epsilon$, $\epsilon \sim \mathcal{N}(0, \mathbf{I})$. This equation yield a way to predict \mathbf{x}_0 at each time step using the predicted noise ϵ_θ as:

$$\tilde{\mathbf{x}}_0(\mathbf{x}_t) = (\mathbf{x}_t - \sqrt{1 - \bar{\alpha}_t} \cdot \epsilon_\theta(\mathbf{x}_t, t)) / \sqrt{\bar{\alpha}_t}. \quad (6)$$

The reconstruction loss is typically defined as the Mean Squared Error (MSE) between the prediction $\tilde{\mathbf{x}}_0$ and data \mathbf{x}_0 . However, when we reframe the Layout generation as a continuous diffusion process, the results often exhibit poor global alignment and undesirable overlaps. This phenomenon occurs because the diffusion loss and the FID metric are not sensitive to minor variations in coordinates, yet they can cause tangible differences in visual quality. Since the contiuous search space for geometric attributes is much larger than in a discrete diffusion model, the diffusion loss holds many local minimums with similar FIDs and varying alignment scores. To address these issues, we propose to combine two additional aesthetic constraints in the reconstruction loss:

$$\mathcal{L}_{\text{rec}} = \text{MSE}(\tilde{\mathbf{x}}_0, \mathbf{x}_0) + \omega_t \cdot (\mathcal{C}_{\text{alg}}(\tilde{\mathbf{x}}_0(\mathbf{x}_t), \mathbf{x}_0) + \mathcal{C}_{\text{olp}}(\tilde{\mathbf{x}}_0(\mathbf{x}_t))), \quad (7)$$

where ω_t is a time-dependent weight to prevent convergence to local minimum. \mathcal{C}_{olp} is the overlap constraint function, while \mathcal{C}_{alg} can refer to either the local or global alignment constraint (represented as $\mathcal{C}_{\text{l-alg}}$, $\mathcal{C}_{\text{g-alg}}$), which will be defined below.

Alignment constraint The alignment loss (Li et al., 2020) is a common metric to evaluate the alignment between layout elements for aesthetics assessment. While calculating this metric, bounding boxes are denoted by its six coordinates $\mathbf{b}_i = (b_i^L, b_i^{XC}, b_i^R, b_i^T, b_i^{YC}, b_i^B)$ corresponds to six possible alignment types: (L), X-center (XC), right (R), top (T), Y-center (YC), and bottom (B) alignment. Since this loss function promotes an alignment pattern where each element is aligned with just one other element based on one type, we term it *local alignment* loss. For a set of l bounding boxes $\mathbf{b}_1, \dots, \mathbf{b}_l$ in a layout \mathbf{x} , the local alignment loss is defined as:

$$\mathcal{C}_{\text{l-alg}}(\mathbf{x}) = \sum_{i=1}^l \min \begin{pmatrix} g(\Delta b_i^L), & g(\Delta b_i^{XC}), & g(\Delta b_i^R) \\ g(\Delta b_i^T), & g(\Delta b_i^{YC}), & g(\Delta b_i^B) \end{pmatrix}, \quad (8)$$

where $g(x) = -\log(1 - x)$, $\Delta b_i^* = \min_{j \neq i} |b_i^* - b_j^*|$, $* \in \mathcal{A} = \{\text{L, XC, R, T, YC, B}\}$, and the minimum of the matrix above is defined as the smallest value among all its elements.

However, local alignment pattern is inconsistent with alignment observed in real-world graphic designs. For instance, in the context of website layouts, there exist elements that do not align with any others, while in publication layouts, certain elements might align with multiple others in multiple ways.

In order to encourage global alignment of elements, we propose a novel alignment loss function that encourages the model to learn global alignment pattern in the real data using an alignment mask. Specifically, for each of the six alignment types, we define the coordinate difference matrix for a layout \mathbf{x} as $\mathbf{A}^*(\mathbf{x})_{i,j} = |b_i^* - b_j^*|$, $* \in \mathcal{A}$. Then the alignment loss function between a given prediction $\tilde{\mathbf{x}}$ at time t and a real layout \mathbf{x} is defined as:

$$\mathcal{C}_{\text{g-alg}}(\tilde{\mathbf{x}}, \mathbf{x}) = -\log \left(1 - \frac{1}{6} \sum_{* \in \mathcal{A}} \frac{\|\mathbf{A}^*(\tilde{\mathbf{x}}) \circ \mathbf{1}_{\mathbf{A}^*(\mathbf{x})=0}\|_1}{\|\mathbf{1}_{\mathbf{A}^*(\mathbf{x})=0}\|_1} \right), \quad (9)$$

where $\mathbf{1}_{\mathbf{A}^*(\mathbf{x})=0}$ is the binary ground truth alignment mask matrix selecting the zero entries of the coordinate difference matrix of the true layout, which represents the true alignment pattern in \mathbf{x} , and \circ is the Hadamard product.

Overlap constraint To prevent overlapping elements in the generated layout, $\tilde{\mathbf{x}}$, we apply a mean pairwise intersection over union loss function, characterized by the pairwise IoU matrix, $\mathbf{O}(\mathbf{x})_{ij} = (\mathbf{b}_i \cap \mathbf{b}_j) / (\mathbf{b}_i \cup \mathbf{b}_j)$. This function monotonically identifies similarities between sets but it has a continuous plane of stationary points, corresponding to the cases when a bounding box is fully contained within another. In such situations, infinitesimal adjustments to the bounding boxes do not cause the enclosed box to exceed the boundary of the larger box. To further penalize aforementioned instances, we define another matrix using the distance between centers of boxes, $\mathbf{D}(\mathbf{x})_{i,j} = e^{-\sqrt{(b_i^{\text{XC}} - b_j^{\text{XC}})^2 + (b_i^{\text{YC}} - b_j^{\text{YC}})^2}}$, which has value range from 0 to 1. Then we combine it with a mask matrix selecting overlapping pairs using the pairwise IoU matrix. The overlap constraint function is given as:

$$\mathcal{C}_{\text{olp}}(\tilde{\mathbf{x}}) = \text{mean}(\mathbf{O}(\tilde{\mathbf{x}}) + \mathbf{D}(\tilde{\mathbf{x}}) \circ \mathbf{1}_{\mathbf{O}(\tilde{\mathbf{x}}) \neq 0}). \quad (10)$$

Minimizing the $\mathbf{D}(\mathbf{x})$ term push elements away from each other when one is entirely encompassed by another and for disjoint element pairs, the mask $\mathbf{1}_{\mathbf{x} \neq 0}$ deactivates the divisive affect.

Time-dependent constraint weight In our observations, directly applying the alignment and overlap loss to noisy layout hinders the faithful reconstruction. This is due to the constraint function introducing numerous local minima within the parameter space as demonstrated in Figure B.2. To mitigate this, we employ a series of time-dependent constraint weight to enforce the constraint only for smaller time t to finetune the misaligned coordinates in a less noisy prediction $\tilde{\mathbf{x}}_0$. We empirically choose $\omega_t = (1 - \bar{\alpha}_t)$ of a constant β schedule as the constraint weight series. A detailed explanation and illustration is provided in Appendix B.1.

Post-processing The model exhibited enhanced performance across FID, alignment, and Max-IoU metrics when trained with constraints. However, LACE may generate layouts with minor misalignment as the coordinate searching space is much larger than that of the discrete diffusion model. Fortunately, further refinement of its visual quality is straightforward and efficient. Guided by the strategies outlined in (Kikuchi et al., 2021), we employ constraint optimization in the post-processing phase, focusing on global alignment and, when suitable, the overlap constraint, targeting the geometric attributes directly. The application of global alignment demands an alignment mask, selecting coordinate pairs for minimization. In training, this mask is calculated using training data, ensuring the accurate learning of human-designed alignment patterns, as introduced in Eq. (9). Since there are no ground truth in the inference post-processing stage, we propose to use a threshold δ to identify nearly aligned entries in the coordinate difference matrix of the produced layout. Thus, the post-process forces elements to align with each other based on the pattern inferred from the raw output. It should be noted that an excessively large threshold will force more alignment, erasing the subtle structure of a layout and leading to coarse or even collapsing generation. A small threshold, on the other hand, might be ineffective in inducing modifications. Thus, the raw outputs must have a low coordinate difference in misaligned entries. In our experiment we set δ equal to 1/64 of the scaled canvas range, as explained in Appendix B.2.

3 RELATED WORK

Layout Generation Various automatic layout generation methods have emerged to aid the efficient creation of visually attractive and organized content across digital and print mediums, including websites, magazines, and mobile apps. Early works (O’Donovan et al., 2014; O’Donovan et al.,

2015) create layouts by optimizing energy-based objectives derived from design principles. With the advent of deep generative models, data-driven models LayoutGAN (Li et al., 2020) and LayoutVAE (Jyothi et al., 2019) are developed and enables more flexible conditional layout generation. LayoutGAN++ (Kikuchi et al., 2021) improves the performance of LayoutGAN for unconditional layout generation and proposes a CLG-LO framework to optimize a pre-trained LayoutGAN++ model to fulfill aesthetic constraints. LayoutTransformer (Gupta et al., 2021) and VTN (Arroyo et al., 2021) are autoregressive models based on transformer architectures, they improve the generation diversity and quality. However, the autoregressive mechanism hinders their application on conditional generation. BLT (Kong et al., 2022) introduces a bidirectional transformer encoder similar to masked language models to facilitate conditional generation with transformer models. However, the BLT model requires specifying the number of elements in advance. Thus, it can not solve completion tasks based on partial layout. LayoutFormer++ (Jiang et al., 2023) introduces a decoding strategy in its transformer encoder-decoder architecture to enable high-quality, conditional layout generation in an autoregressive manner. However, its backtracking mechanism may necessitate multiple reversions in the decoding process to rectify any invalid generations. Additionally, retraining is necessary for adapting to different conditional tasks. Zheng et al. (2019) incorporated image and text features into their layout generation model to achieve content-awareness.

Diffusion-based layout generation Recently, diffusion models have been adopted to develop unified models that adapt to various conditions and improve generation quality. PLay (Cheng et al., 2023) uses a latent diffusion model to generate layout conditioned on guidelines—lines align elements. LayoutDM (Inoue et al., 2023) and LDGM (Hui et al., 2023) build a unified model for various generation conditions without guidelines using the discrete diffusion (Austin et al., 2021) framework. They independently developed the same attribute-specific corruption strategy to restrict variables of different attributes to their respective sample spaces in the mask-and-replace forward process (Gu et al., 2022). In addition, LDGM employs discretized Gaussian noise to facilitate gradual coordinate changes. LayoutDiffusion (Zhang et al., 2023), adopting a similar design to LDGM, enhances visual quality of three generation tasks significantly by using a larger transformer backbone, particularly improving alignment and overlap metrics. In contrast, our method aims to enhance visual quality by applying constraint functions without scaling up the network architecture. Motivated by the superior performance of DDPM (Ho et al., 2020) in image generation, two recent studies have aimed to generate layouts in a continuous space. A diffusion-based model for unconditional generation was proposed by (He et al., 2023). Although it generate embedding vectors in continuous space, geometric attributes are quantized to discrete tokens, thus, is not differentiable. Another work (Chai et al., 2023) adopt DDPM for conditional generation that directly generate continuous geometric attributes (size and position) based on given categorical attributes. Because the noisy attributes share the same continuous sample space, DDPM-based models do not need the attribute-specific corruption strategy. Our model further innovates by directly generating geometric and categorical attributes in continuous space and utilizing differentiable aesthetic constraint functions to enhance generation quality. In addition, we train diffusion models using both masked and unmasked layouts similar to DiffMAE (Wei et al., 2023) to unify various tasks in a single model.

4 EXPERIMENTS

4.1 EXPERIMENT SETUP

Datasets We use two large-scale datasets for comparison. PubLayNet (Zhong et al., 2019) consists of 330K document layouts with five class element annotation retrieved from articles from PubMed CentraTM. Rico (Deka et al., 2017) consists of 72k user interfaces designs from 9.7k Android apps spanning 27 classes. Following LayoutDM (Inoue et al., 2023), for both datasets, we discard instance that has more than 25 elements, and pad the remaining layouts to a unified maximum length of 25. For Rico dataset, we use layouts that has only the most frequent 25 classes. The refined PubLayNet and Rico datasets were then split into training, validation, and test sets containing 315, 757/16, 619/11, 142 and 35, 851/2, 109/4, 218 samples respectively.

Evaluation Metrics To assess the quality of generation, we employ four computational metrics. (1) Fréchet Inception Distance (FID) (Heusel et al., 2017) compute the distance between the feature distributions of generated and real layout in the feature space of a pre-trained feature extraction

model. It evaluate both fidelity and diversity of generative models. We employ the same feature extraction model used in LayoutDM to compute FID. (2) Maximum Intersection-over-Union (Max.) is a metric for conditional generation. It compute the average IoU between optimally matched pairs of elements from two layouts that contain elements with identical category sets. (3) Alignment (Align.) and (4) Overlap is used for aesthetics assessment which compute the normalized alignment score. We adopt the implementation of all metrics as proposed in LayoutGAN++ (Kikuchi et al., 2021).

Generation Tasks We train a unified model for five generation tasks defined in previous works (Gupta et al., 2021; Jiang et al., 2022; Rahman et al., 2021) including unconditional generation (**U-Cond**), conditional generation based solely on class (**C→S+P**), conditional generation based on both class and size (**C+S→P**) of each element, **completion** with attributes given for a subset of elements, and **refinement** of a noisy layout. For completion task, following LayoutDM (Inoue et al., 2023), we randomly sample 0% to 20% of elements from real samples as the binary condition mask. In the completion task, we follow LayoutDM ((Inoue et al., 2023)), where we create a binary condition mask by randomly sampling between 0% and 20% of elements from real samples. In the refinement task, following RUIITE ((Rahman et al., 2021)), we introduce minor Gaussian noise to the size and position of each element, characterized by a mean of 0 and a variance of 0.01, to simulate a perturbed layout. For more implementation details, please see Appendix B.

4.2 QUANTITATIVE RESULTS

We benchmark our method, LACE, against several state-of-the-art (SOTA) models on five generation tasks using the PubLayNet and Rico datasets. These models are categorized into traditional and diffusion-based models. Traditional models are further split into task-specific models, which include

PubLayNet		Task	C→S+P		C+S→P		Completion		U-Cond	
Model	Metric		FID↓	Max.↑	FID↓	Max.↑	FID↓	Max.↑	FID↓	Align.↓
Task-specific models										
LayoutVAE			26.0	0.316	27.5	0.315	-	-	-	-
NDN-none			61.1	0.162	69.4	0.222	-	-	-	-
LayoutGAN++			24.0	0.263	9.94	0.342	-	-	-	-
Task-agnostic models										
LayoutTrans			14.1	0.272	16.9	0.320	8.36	0.451	13.9	0.127
BLT			72.1	0.215	5.10	0.387	131	0.345	116	0.153
BART			9.36	0.320	5.88	0.375	9.58	0.446	16.6	0.116
MaskGIT			17.2	0.319	5.86	0.380	19.7	0.484	27.1	0.101
Diffusion-based models										
VQDiffusion			10.3	0.319	7.13	0.374	11.1	0.373	15.4	0.193
LayoutDM			7.95	0.310	4.25	0.381	7.65	0.377	13.9	0.195
LACE (local)			4.88	0.331	2.80	0.437	5.86	0.401	8.45	0.141
LACE (global)			5.14	0.383	3.07	0.463	6.03	0.396	8.35	0.185
LACE (local) w/ post			4.63	0.390	2.69	0.462	5.90	0.399	8.47	0.032
LACE (global) w/ post			4.56	0.388	2.53	0.463	5.63	0.394	7.43	0.074
Validation data			6.25	0.438	6.25	0.438	6.25	0.438	6.25	0.021
Rico		Task	C→S+P		C+S→P		Completion		U-Cond	
Model	Metric		FID↓	Max.↑	FID↓	Max.↑	FID↓	Max.↑	FID↓	Align.↓
Task-specific models										
LayoutVAE			33.3	0.249	30.6	0.283	-	-	-	-
NDN-none			28.4	0.158	62.8	0.219	-	-	-	-
LayoutGAN++			6.84	0.267	6.22	0.348	-	-	-	-
Task-agnostic models										
LayoutTrans			5.57	0.223	3.73	0.323	3.71	0.537	7.63	0.068
BLT			17.4	0.202	4.48	0.340	117	0.471	88.2	1.030
BART			3.97	0.253	3.18	0.334	8.87	0.527	11.9	0.090
MaskGIT			26.1	0.262	8.05	0.320	33.5	0.533	52.1	0.015
Diffusion-based models										
VQDiffusion			4.34	0.252	3.21	0.331	11.0	0.541	7.46	0.178
LayoutDM			3.55	0.277	2.22	0.392	9.00	0.576	6.65	0.162
LACE (local)			3.31	0.336	2.66	0.418	5.09	0.518	4.71	0.107
LACE (global)			3.24	0.340	2.87	0.418	4.45	0.527	4.63	0.117
LACE (local) w/ post			2.88	0.347	2.17	0.430	3.82	0.539	3.99	0.031
LACE (global) w/ post			3.24	0.344	2.16	0.428	4.30	0.540	4.51	0.035
Validation data			1.85	0.691	1.85	0.691	1.85	0.691	1.85	0.109

Table 1: Quantitative results on PubLayNet and Rico for four generation tasks. The top two results are highlighted with deep and light red shades, respectively.

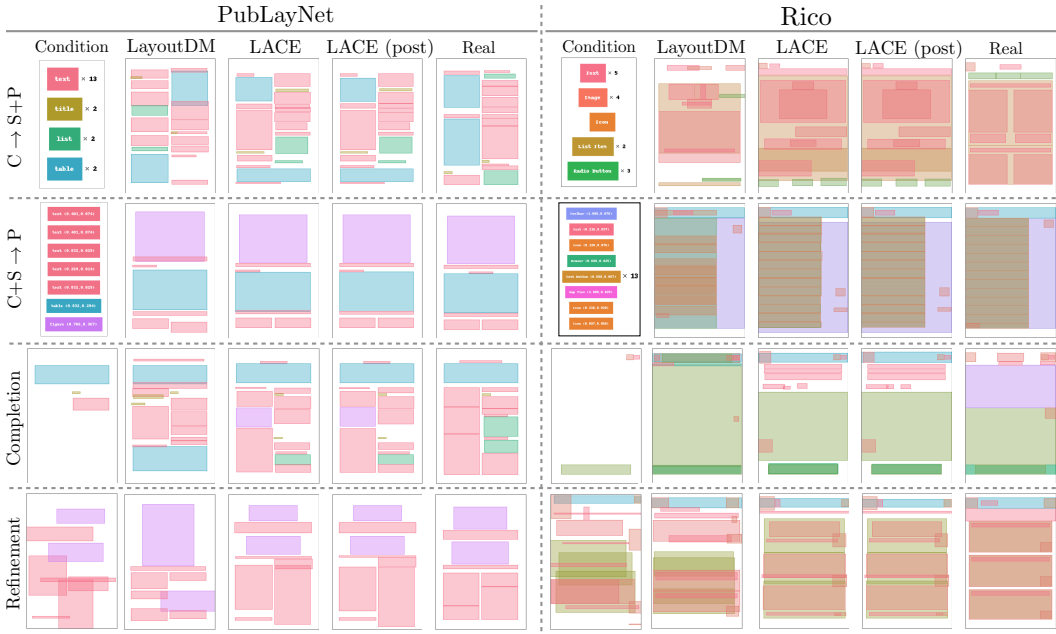


Figure 3: Qualitative comparison between LACE and LayoutDM in conditional generation tasks.

LayoutVAE (Jyothi et al., 2019), NDN-none (Lee et al., 2020), LayoutGAN++ (Kikuchi et al., 2021), and RUIITE (Rahman et al., 2021), and task-agnostic models like LayoutTrans (Gupta et al., 2021), BLT (Kong et al., 2022), and MaskGIT (Chang et al., 2022). On the other hand, the diffusion-based models considered are VQDiffusion (Gu et al., 2022) and LayoutDM (Inoue et al., 2023). For evaluating unconditional generation, we utilize FID and Alignment metrics. Meanwhile, for refinement and conditional generation based on partial attributes, we apply FID and MaxIoU. Since the overlap pattern is prevalent in the Rico dataset, we only apply the overlap constraint during training on the PubLayoutNet dataset. Therefore the overlap metric is only used in experiments on the PubLayoutNet dataset. Furthermore, results from models using both local and global alignment constraints are reported in the benchmark experiments. In the post-processing stage, we optimize the global alignment using the δ -alignment mask introduced in section 2.3.

Conditional and Unconditional Generation We demonstrate that LACE, even without post-processing, achieves state-of-the-art (SOTA) performance in four tasks including unconditional and conditional generation given partial attributes. LACE surpasses other models that utilize discrete diffusion in benchmark experiments conducted on the Rico and PubLayoutNet datasets. The results for LACE, along with nine baseline methods, are presented in Table 1 and Appendix A. We observed Both LACE versions, using local and global alignment constraints, show similar performance. LACE (global) exhibited superior performance on the PubLayoutNet dataset, possibly due to the greater prevalence of alignment patterns in PubLayoutNet. The results of LACE with post-processing show a significant improvement in alignment, while either maintaining or slightly enhancing the FID. This is attributed to the adjustments that fine-tune the alignment without substantially altering the global organization of elements. Figure.3 shows the qualitative comparison results between LACE and LayoutDM for conditional generation. Additional qualitative results are in the Appendix C.

Refinement Continuous diffusion using Gaussian noise is naturally an expert at refining noisy layouts because noisy layouts can be viewed as noisy states during the forward process. And the continuous diffusion model is trained to reverse the corruption. Since it is only beneficial to refine a layout that is clear enough to show the relative position of elements, we assume the noise level of the input matches the noise states at time step τ , where the time-dependent constraint weight starts to encourage the importance of the constraint functions ($\omega_t = 0.1$). Thus, we use a fixed LACE model to refine a noisy layout, treat the input as a noisy state at time τ , and start a partial reverse process to refine it. The results shown in Table 2 demonstrate LACE outperforms competing models, achieving FID and MaxIoU scores comparable to that of LACE with post-processing.

Model	Dataset	Rico		PubLayNet	
		FID↓	Max↑	FID↓	Max↑
Task-specific models					
RUIITE (Rahman et al., 2021)		263.23	0.421	6.39	0.415
Task-agnostic models					
Noisy input		134	0.213	130	0.242
LayoutDM		2.77	0.370	4.25	0.381
LACE (local)		1.79	0.485	1.65	0.491
Post-processed					
LACE (local)		1.76	0.484	1.80	0.500
Validation data		6.25	0.438	6.25	0.438

Table 2: Results in the refinement task on PubLayNet and Rico datasets.

4.3 ABLATION STUDY

We conducted an ablation study on the PubLayNet dataset to evaluate the role of aesthetic constraints and masked input during training. We trained a LACE model without aesthetic constraints and three diffusion models with constraints for unconditional generation and two conditional tasks ($C \rightarrow S+P$, $C+S \rightarrow P$). Using the unconditional model, we also applied the in-painting technique (Lugmayr et al., 2022) for completion. We only include LACE using local alignment constraint (noted as LACE w/ \mathcal{C}), in the ablation study, as LACE with both constraints exhibit similar performance. Table 3 displays the results. The result of task-specific models is comparable to LACE, which proves the effectiveness of our task unification method. LACE achieves a much lower alignment score and slightly reduced FID compared to LACE without aesthetic constraints, suggesting the effectiveness of constraint optimization. In addition, the post-process notably improves the alignment in unconditional generation without sacrificing the FID score. However, the post-process is not as effective for LACE without constraints. A possible explanation is the coordinate difference in the raw output is too large for the threshold to detect, resulting in a smaller number of coordinate differences being minimized. We include detailed alignment and overlap results in Appendix A.

Task	Metric	Task-specific w/ \mathcal{C}	LACE w/o \mathcal{C}	LACE	LACE w/o \mathcal{C} w/ post	LACE w/ post
U-Cond	FID↓	6.76	8.70	8.45	10.31	8.47
	Align↓	0.128	0.238	0.141	0.215	0.032
$C \rightarrow S+P$	FID↓	6.12	5.08	4.88	4.76	4.63
	Max↑	0.386	0.383	0.332	0.389	0.390
$C+S \rightarrow P$	FID↓	2.25	3.21	2.80	2.57	2.69
	Max↑	0.478	0.460	0.437	0.461	0.462
Completion	FID↓	7.73*	6.42	5.86	6.01	5.90
	Max↑	0.399 *	0.403	0.401	0.385	0.399

Table 3: Results of the ablation study conducted on the PubLayNet dataset. The asterisk (*) denotes in-painting results using the unconditional model. Symbol \mathcal{C} represents ‘constraints’, while ‘post’ refers to post-processing. The top two results are highlighted in deep and light red shades.

5 CONCLUSIONS

We introduced LACE, a diffusion a unified model for controllable layout generation in a continuous state space. Using the diffusion framework with alignment and overlap loss constraints, LACE outperforms previous state-of-the-art baselines in both FID and visual quality. Efficient post-processing can further improve generation quality regarding alignment and overlap, without sacrificing FID. While LACE demonstrates advancements in layout generation, it has several limitations. First, it restricts layout elements to box shapes, limiting representation flexibility. Additionally, it lacks background and content awareness, which could be crucial for more context-driven designs. The model also handles only a limited number of elements and relies on a closed label set. These constraints may restrict its applicability in complex, varied design scenarios. For future work, adopting arbitrary shapes can better mirror real-world graphic design scenarios as most existing work relies on rectangular boxes for element representation. In addition, using images or text as conditions to generate a more relevant layout for the content should improve the performance of downstream tasks, such as layout-guided image generation and automated web design.

ACKNOWLEDGEMENT

This work is partially supported by NSF AI Institute-2229873, NSF RI-2223292, an Amazon research award, and an Adobe gift fund. Any opinions, findings and conclusions or recommendations expressed in this material are those of the author(s) and do not necessarily reflect the views of the National Science Foundation, the Institute of Education Sciences, or the U.S. Department of Education.

REFERENCES

- Diego Martin Arroyo, Janis Postels, and Federico Tombari. Variational transformer networks for layout generation. In *Proceedings of the IEEE/CVF Conference on Computer Vision and Pattern Recognition*, pp. 13642–13652, 2021.
- Jacob Austin, Daniel D Johnson, Jonathan Ho, Daniel Tarlow, and Rianne Van Den Berg. Structured denoising diffusion models in discrete state-spaces. *Advances in Neural Information Processing Systems*, 34:17981–17993, 2021.
- Shang Chai, Liansheng Zhuang, and Fengying Yan. Layoutdm: Transformer-based diffusion model for layout generation. In *Proceedings of the IEEE/CVF Conference on Computer Vision and Pattern Recognition*, pp. 18349–18358, 2023.
- Huiwen Chang, Han Zhang, Lu Jiang, Ce Liu, and William T Freeman. Maskgit: Masked generative image transformer. In *Proceedings of the IEEE/CVF Conference on Computer Vision and Pattern Recognition*, pp. 11315–11325, 2022.
- Chin-Yi Cheng, Forrest Huang, Gang Li, and Yang Li. Play: Parametrically conditioned layout generation using latent diffusion. *arXiv preprint arXiv:2301.11529*, 2023.
- Biplab Deka, Zifeng Huang, Chad Franzen, Joshua Hirschman, Daniel Afergan, Yang Li, Jeffrey Nichols, and Ranjitha Kumar. Rico: A mobile app dataset for building data-driven design applications. In *Proceedings of the 30th annual ACM symposium on user interface software and technology*, pp. 845–854, 2017.
- Vincent Dumoulin, Jonathon Shlens, and Manjunath Kudlur. A learned representation for artistic style. In *International Conference on Learning Representations*, 2017.
- William Feller. On the theory of stochastic processes, with particular reference to applications. In *Selected Papers I*, pp. 769–798. Springer, 2015.
- Ian Goodfellow, Jean Pouget-Abadie, Mehdi Mirza, Bing Xu, David Warde-Farley, Sherjil Ozair, Aaron Courville, and Yoshua Bengio. Generative adversarial nets. *Advances in neural information processing systems*, 27, 2014.
- Shuyang Gu, Dong Chen, Jianmin Bao, Fang Wen, Bo Zhang, Dongdong Chen, Lu Yuan, and Baining Guo. Vector quantized diffusion model for text-to-image synthesis. In *Proceedings of the IEEE/CVF Conference on Computer Vision and Pattern Recognition*, pp. 10696–10706, 2022.
- Kamal Gupta, Justin Lazarow, Alessandro Achille, Larry S Davis, Vijay Mahadevan, and Abhinav Shrivastava. Layouttransformer: Layout generation and completion with self-attention. In *Proceedings of the IEEE/CVF International Conference on Computer Vision*, pp. 1004–1014, 2021.
- Xizewen Han, Huangjie Zheng, and Mingyuan Zhou. Card: Classification and regression diffusion models. *Advances in Neural Information Processing Systems*, 35:18100–18115, 2022.
- Liu He, Yijuan Lu, John Corring, Dinei Florencio, and Cha Zhang. Diffusion-based document layout generation. *arXiv preprint arXiv:2303.10787*, 2023.
- Martin Heusel, Hubert Ramsauer, Thomas Unterthiner, Bernhard Nessler, and Sepp Hochreiter. Gans trained by a two time-scale update rule converge to a local nash equilibrium. *Advances in neural information processing systems*, 30, 2017.
- Jonathan Ho, Ajay Jain, and Pieter Abbeel. Denoising diffusion probabilistic models. *Advances in Neural Information Processing Systems*, 33:6840–6851, 2020.
- Mude Hui, Zhizheng Zhang, Xiaoyi Zhang, Wenzuan Xie, Yuwang Wang, and Yan Lu. Unifying layout generation with a decoupled diffusion model. In *Proceedings of the IEEE/CVF Conference on Computer Vision and Pattern Recognition*, pp. 1942–1951, 2023.

- Naoto Inoue, Kotaro Kikuchi, Edgar Simo-Serra, Mayu Otani, and Kota Yamaguchi. Layoutdm: Discrete diffusion model for controllable layout generation. In *Proceedings of the IEEE/CVF Conference on Computer Vision and Pattern Recognition (CVPR)*, pp. 10167–10176, June 2023.
- Zhaoyun Jiang, Huayu Deng, Zhongkai Wu, Jiaqi Guo, Shizhao Sun, Vuksan Mijovic, Zijiang Yang, Jian-Guang Lou, and Dongmei Zhang. Unilayout: Taming unified sequence-to-sequence transformers for graphic layout generation. *arXiv preprint arXiv:2208.08037*, 2022.
- Zhaoyun Jiang, Jiaqi Guo, Shizhao Sun, Huayu Deng, Zhongkai Wu, Vuksan Mijovic, Zijiang James Yang, Jian-Guang Lou, and Dongmei Zhang. Layoutformer++: Conditional graphic layout generation via constraint serialization and decoding space restriction. In *Proceedings of the IEEE/CVF Conference on Computer Vision and Pattern Recognition*, pp. 18403–18412, 2023.
- Akash Abdu Jyothi, Thibaut Durand, Jiawei He, Leonid Sigal, and Greg Mori. Layoutvae: Stochastic scene layout generation from a label set. In *Proceedings of the IEEE/CVF International Conference on Computer Vision*, pp. 9895–9904, 2019.
- Kotaro Kikuchi, Edgar Simo-Serra, Mayu Otani, and Kota Yamaguchi. Constrained graphic layout generation via latent optimization. In *Proceedings of the 29th ACM International Conference on Multimedia*, pp. 88–96, 2021.
- Diederik P Kingma and Max Welling. Auto-encoding variational bayes. *arXiv preprint arXiv:1312.6114*, 2013.
- Xiang Kong, Lu Jiang, Huiwen Chang, Han Zhang, Yuan Hao, Haifeng Gong, and Irfan Essa. Blt: bidirectional layout transformer for controllable layout generation. In *European Conference on Computer Vision*, pp. 474–490. Springer, 2022.
- Hsin-Ying Lee, Lu Jiang, Irfan Essa, Phuong B Le, Haifeng Gong, Ming-Hsuan Yang, and Weilong Yang. Neural design network: Graphic layout generation with constraints. In *Computer Vision–ECCV 2020: 16th European Conference, Glasgow, UK, August 23–28, 2020, Proceedings, Part III 16*, pp. 491–506. Springer, 2020.
- Jianan Li, Jimei Yang, Jianming Zhang, Chang Liu, Christina Wang, and Tingfa Xu. Attribute-conditioned layout gan for automatic graphic design. *IEEE Transactions on Visualization and Computer Graphics*, 27(10):4039–4048, 2020.
- Andreas Lugmayr, Martin Danelljan, Andres Romero, Fisher Yu, Radu Timofte, and Luc Van Gool. Repaint: Inpainting using denoising diffusion probabilistic models. In *Proceedings of the IEEE/CVF Conference on Computer Vision and Pattern Recognition*, pp. 11461–11471, 2022.
- Peter O’Donovan, Aseem Agarwala, and Aaron Hertzmann. Designscape: Design with interactive layout suggestions. In *Proceedings of the 33rd annual ACM conference on human factors in computing systems*, pp. 1221–1224, 2015.
- Peter O’Donovan, Aseem Agarwala, and Aaron Hertzmann. Learning layouts for single-pagegraphic designs. *IEEE transactions on visualization and computer graphics*, 20(8):1200–1213, 2014.
- Xufang Pang, Ying Cao, Rynson WH Lau, and Antoni B Chan. Directing user attention via visual flow on web designs. *ACM Transactions on Graphics (TOG)*, 35(6):1–11, 2016.
- Soliha Rahman, Vinoth Pandian Sermuga Pandian, and Matthias Jarke. Ruite: Refining ui layout aesthetics using transformer encoder. In *26th International Conference on Intelligent User Interfaces-Companion*, pp. 81–83, 2021.
- Jiaming Song, Chenlin Meng, and Stefano Ermon. Denoising diffusion implicit models. *arXiv preprint arXiv:2010.02502*, 2020.
- Ashish Vaswani, Noam Shazeer, Niki Parmar, Jakob Uszkoreit, Llion Jones, Aidan N Gomez, Łukasz Kaiser, and Illia Polosukhin. Attention is all you need. *Advances in neural information processing systems*, 30, 2017.
- Chen Wei, Karttikeya Mangalam, Po-Yao Huang, Yanghao Li, Haoqi Fan, Hu Xu, Huiyu Wang, Cihang Xie, Alan Yuille, and Christoph Feichtenhofer. Diffusion models as masked autoencoders. *arXiv preprint arXiv:2304.03283*, 2023.
- Yong-Liang Yang, Jun Wang, Etienne Vouga, and Peter Wonka. Urban pattern: Layout design by hierarchical domain splitting. *ACM Transactions on Graphics (TOG)*, 32(6):1–12, 2013.

Junyi Zhang, Jiaqi Guo, Shizhao Sun, Jian-Guang Lou, and Dongmei Zhang. Layoutdiffusion: Improving graphic layout generation by discrete diffusion probabilistic models. *arXiv preprint arXiv:2303.11589*, 2023.

Xinru Zheng, Xiaotian Qiao, Ying Cao, and Rynson WH Lau. Content-aware generative modeling of graphic design layouts. *ACM Transactions on Graphics (TOG)*, 38(4):1–15, 2019.

Xu Zhong, Jianbin Tang, and Antonio Jimeno Yepes. Publaynet: largest dataset ever for document layout analysis. In *2019 International Conference on Document Analysis and Recognition (ICDAR)*, pp. 1015–1022. IEEE, 2019.

A ADDITIONAL ABLATION RESULTS

We compared LACE with LayoutDM and LayoutGAN++ in terms of overlap and alignment. LayoutGAN++ is a task-specific model that also uses constraints in training and post-processing. We directly adopt their results in the original paper. In addition, we apply post-processing to LayoutDM to demonstrate the advantage in using constraint during training for diffusion model. Results are shown in Table A.1 and Table A.2. Both LayoutDM and LayoutGAN++ show a notable FID increase after post-processing. In contrast, LACE maintains a stable FID and achieves lower overlap and alignment scores before post-processing, which are further improved afterward.

Model	Metric	Task		
		FID↓	Align↓	C→S+P Overlap.↓
Task-specific models				
NDN-none		61.1	0.350	16.5
LayoutGAN++		24.0	0.190	22.80
LayoutGAN++ w/ \mathcal{C}		22.3	0.160	14.27
LayoutGAN++ w/ \mathcal{C} & post		26.2	0.160	1.18
Diffusion-based models				
LayoutDM		7.95	0.106	16.43
LayoutDM w/ post		15.2	0.083	6.076
LACE w/o \mathcal{C}		6.12	0.054	1.636
LACE (local)		4.88	0.043	1.638
LACE (global)		5.14	0.046	1.791
LACE (local) w/ post		4.63	0.010	1.211
LACE (global) w/ post		4.56	0.009	0.906
Validation data		6.25	0.021	0.117

Table A.1: FID, overlap and alignment results in the C→S+P task on the PubLayNet dataset.

Additionally, LACE, even without post-processing, outperforms LayoutDM with post-processing in alignment and overlap scores. This serves as proof of the effectiveness of the constraint loss in our approach.

Model	Metric	Task		C+S→P		Completion		U-Cond	
		Align↓	Overlap.↓	Align↓	Overlap.↓	Align↓	Overlap.↓	Align↓	Overlap.↓
Diffusion-based models									
LayoutDM		0.119	18.91	0.107	15.04	0.195	13.43		
LayoutDM w/ post		0.117	6.506	0.073	5.220	0.200	4.641		
LACE w/o \mathcal{C}		0.065	3.062	0.054	3.223	0.238	7.533		
LACE (local)		0.061	3.309	0.040	2.772	0.141	3.615		
LACE (global)		0.061	3.439	0.042	3.056	0.185	4.140		
LACE (local) w/ post		0.016	1.400	0.014	1.723	0.032	0.586		
LACE (global) w/ post		0.017	1.363	0.017	1.573	0.074	0.768		
Validation data		0.021	0.117	0.021	0.117	0.021	0.117		

Table A.2: Overlap and alignment results on PubLayNet for three generation tasks.

B IMPLEMENTATION SPECIFICATIONS

B.1 TIME-DEPENDENT CONSTRAINT WEIGHT

The time-dependent constraint weight is critical for effective model convergence and output quality. Without this weight, the model struggles to converge, leading to a high Fréchet Inception Distance (FID) score, typically remaining above 100, which indicates poor layout quality. We choose $\omega_t = (1 - \bar{\alpha}_t)$ of a constant β schedule as the constraint weight series. The β schedule is set empirically such that the weight activates the constraint only when t is small when the corruption process has not introduced too much overlap, as demonstrated in Figure B.1. Thus, in the reverse process, the coarse structure of the layout has emerged. Figure B.2 demonstrates the local minimum induced by the constraint functions at noisy steps, hindering convergence.

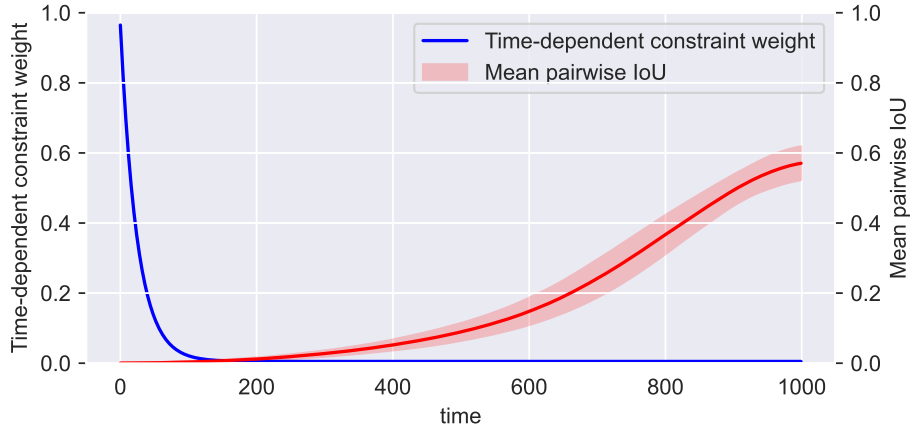


Figure B.1: Time-dependent constraint weight and Mean Pairwise IoU in the forward process.

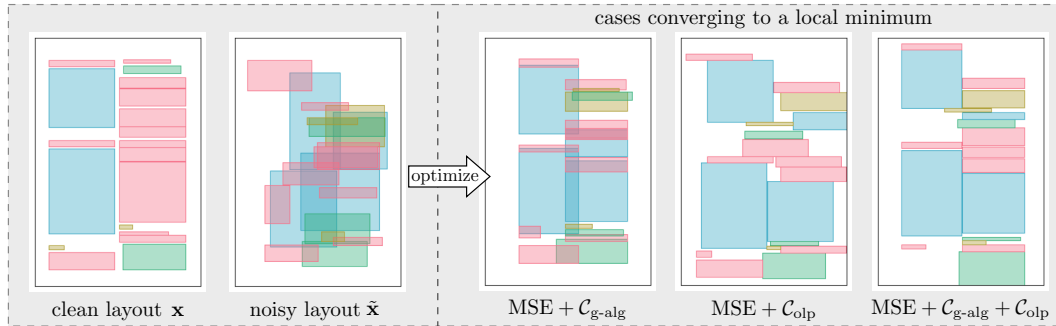


Figure B.2: Examples of convergence to local minimum with alignment and overlap constraints

B.2 POST-PROCESSING THRESHOLD

We use the global alignment and overlap (only on PubLayoutNet) constraints to optimize the raw output of LACE. Since there is no target layout to compute the ground truth alignment mask matrix in Eq. (9), we use a threshold value to compute an alignment mask matrix using the coordinate difference matrix of the generated layout. To determine the threshold for enhanced visual quality post-processing, we first scaled the normalized canvas according to its width/height ratio. We then tested various threshold values, including 1/16, 1/32, 1/64, 1/128, and 1/256. The optimal threshold was empirically determined to be 1/64 of the scaled normalized canvas size. This setting aligns with real dataset observations, where only 0.5% of unaligned coordinate pairs have a smaller difference.

B.3 MODEL ARCHITECTURE

As illustrated in Figure B.3, we adopt a transformer architecture that is implemented in the source code of LayoutDM Inoue et al. (2023) to predict the noise term in Eq. (5). We also choose similar hyper-parameter settings for a fair comparison: 4 layers, 16 attention heads, 2048 hidden dimension in the FNN (feed-forward networks), and the embedding dimension is 1024 for PubLayoutNet and 512 for Rico. In addition, we add two FNNs to encode and decode element vectors. Time embeddings are injected by an modified adaptive layer normalization Dumoulin et al. (2017). Specifically, the layer normalization is:

$$\mathbf{y} = (\mathbf{1} + f_\gamma(\mathbf{v}_t)) \odot \left(\frac{\mathbf{x} - \boldsymbol{\mu}}{\boldsymbol{\sigma}} \right) + f_\beta(\mathbf{v}_t), \quad (\text{B.1})$$

where \mathbf{x} , \mathbf{y} are the input and output of the normalization function, f_γ , f_β are FFN that encode the time-dependent scale and shift, $\boldsymbol{\mu}$, $\boldsymbol{\sigma}$ are \mathbf{x} 's mean and standard deviation, \mathbf{v}_t is the time embedding, $\mathbf{1}$ is a vector of all ones represents a residue connection. \odot is the Hadamard product.

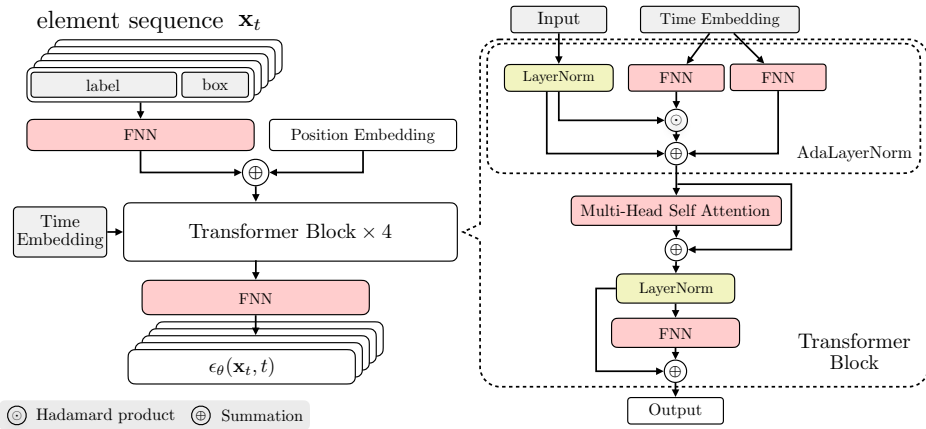


Figure B.3: Neural network architecture for the layout generation diffusion models. The the network takes sequence of layout elements the time variables as input and output the predicted noise. The pink blocks in the figure represent the trainable network components, gray blocks represent input tensors.

B.4 TRAINING DETAILS

We train the model using the Adam optimizer. The batch size is 256. We used a learning rate schedule that included a warmup phase followed by a half-cycle cosine decay. The initial learning rate is set to 0.001. Training is divided into two phases: initially, the model is trained without constraints ($\omega_t = 0$) until convergence is observed in the FID score. In the second phase, constraints are added to the total loss, and training continues until convergence is achieved in both alignment and FID scores. For the Rico dataset, the overlap constraint is excluded due to prevalent overlap patterns in real data. However, in the PubLayNet dataset training, the overlap constraint is applied to prevent undesirable overlaps in publication layouts. The diffusion model employs a total of 1000 forward steps. For efficient generation, we use DDIM sampling with 100 steps.

C QUALITATIVE COMPARISON



Figure C.1: Qualitative comparison between LACE w/ post-processing (left), real (middle), and LayoutDM (right) in conditional generation tasks ($C+S \rightarrow P$) on the PublayNet dataset.



Figure C.2: Qualitative comparison between LACE w/ post-processing (left), real (middle), and LayoutDM (right) in conditional generation tasks ($C+S \rightarrow P$) on the Rico dataset.



Figure C.3: Qualitative comparison between LACE w/ post-processing (left) and LayoutDM (right) in unconditional generation tasks on the PublayNet dataset.



Figure C.4: Qualitative comparison between LACE w/ post-processing (left) and LayoutDM (right) in unconditional generation tasks on the Rico dataset.